JCB Journal of Cell Biology

ARTICLE

The universally conserved GTPase HflX is an RNA helicase that restores heat-damaged *Escherichia coli* ribosomes

Sandip Dey, Chiranjit Biswas, and Jayati Sengupta

The ribosome-associated GTPase HflX acts as an antiassociation factor upon binding to the 50S ribosomal subunit during heat stress in *Escherichia coli*. Although HflX is recognized as a guanosine triphosphatase, several studies have shown that the N-terminal domain 1 of HflX is capable of hydrolyzing adenosine triphosphate (ATP), but the functional role of its adenosine triphosphatase (ATPase) activity remains unknown. We demonstrate that *E. coli* HflX possesses ATP-dependent RNA helicase activity and is capable of unwinding large subunit ribosomal RNA. A cryo–electron microscopy structure of the 50S–HflX complex in the presence of nonhydrolyzable analogues of ATP and guanosine triphosphate hints at a mode of action for the RNA helicase and suggests the linker helical domain may have a determinant role in RNA unwinding. Heat stress results in inactivation of the ribosome, and we show that HflX can restore heat-damaged ribosomes and improve cell survival.

Introduction

HflX, a ribosome-binding GTPase, is classified as a member of the Obg–HflX superfamily (Verstraeten et al., 2011). The Obg-related GTPases, comprising a group of ancient GTPases of the translation factor–related GTPase class, exist in all domains of life (Leipe et al., 2002). Stimulation of the intrinsic GTPase activity of HflX upon interaction with 70S ribosome and ribosomal subunits has been well established (Noble et al., 1993; Shields et al., 2009; Huang et al., 2010; Ash et al., 2012). It has been shown that HflX preferentially binds to the 50S subunit in the presence of GTP (Blombach et al., 2011; Zhang et al., 2015). The protein shares several similarities to bacterial GTPases that interact with the ribosomal subunits, some of which are known to play key roles in ribosome biogenesis (Caldon and March, 2003; Britton, 2009). Thus, HflX has been initially implicated in ribosome biogenesis (Sato et al., 2005; Schaefer et al., 2006). Interestingly, however, although an earlier study (Shields et al., 2009) proposed that HflX functions under stress, recent studies have confirmed that *Escherichia coli* HflX splits 70S ribosomes (Zhang et al., 2015; Coatham et al., 2016) and acts as an antiassociation factor for the 50S subunit in the presence of GTP under heat stress (Zhang et al., 2015).

The crystal structure of *Sulfolobus solfataricus* HflX (Wu et al., 2010) displays two-domain architecture (N-terminal and GTP-binding domains), whereas *E. coli* HflX consists of three domains (Fig. 1 A): well-conserved N-terminal domain 1 (ND1) and 2 (ND2; GTPase domain) followed by an additional C-terminal domain. A fork-like helical domain (termed hereafter as linker helical domain) bridges ND1 and ND2.

Intriguingly, *E. coli* HflX binds and hydrolyzes not only GTP but also ATP upon ribosome binding (Dutta et al., 2009; Jain et al., 2009; Shields et al., 2009; Blombach et al., 2011). A more recent study (Jain et al., 2013) characterized ND1 to be a new ATP-binding domain in *E. coli* HflX, where it was reported to bind and hydrolyze ATP in the presence of 70S ribosome as well as 50S ribosomal subunit. Nevertheless, the functional role of the ATPase activity of HflX remains undefined.

In this study, we elucidate that HflX is an ATP-dependent helicase that exhibits RNA-unwinding activity. Atomic force microscopy (AFM) visualization clearly manifests its affinity and unwinding catalysis on large subunit ribosomal RNA (rRNA) in the presence of ATP. Furthermore, a cryo-EM structure of the 50S–HflX complex in the presence of ATP and GTP illuminates the mechanism of RNA-unwinding action by the protein. Our structural and functional analyses demonstrate a critical role of the linker helical domain in modulating 23S rRNA conformation. Furthermore, in vitro translation and cell survival assays provide clear evidence that HflX is capable of rescuing heat-damaged ribosomes and promoting cell survival after heat stress.

Structural Biology and Bioinformatics Division, Council of Scientific and Industrial Research – Indian Institute of Chemical Biology, Kolkata, India.

Correspondence to: Jayati Sengupta: jayati@iicb.res.in.

© 2018 Dey et al. This article is distributed under the terms of an Attribution–Noncommercial–Share Alike–No Mirror Sites license for the first six months after the publication date (see http://www.rupress.org/terms/). After six months it is available under a Creative Commons License (Attribution–Noncommercial–Share Alike 4.0 International license, as described at https://creativecommons.org/licenses/by-nc-sa/4.0/).

Downloaded from http://rupress.org/jcb/article-pdf/217/7/2519/1608330/jcb_201711131.pdf by guest on 05 December 2025

Check for updates

https://doi.org/10.1083/jcb.201711131

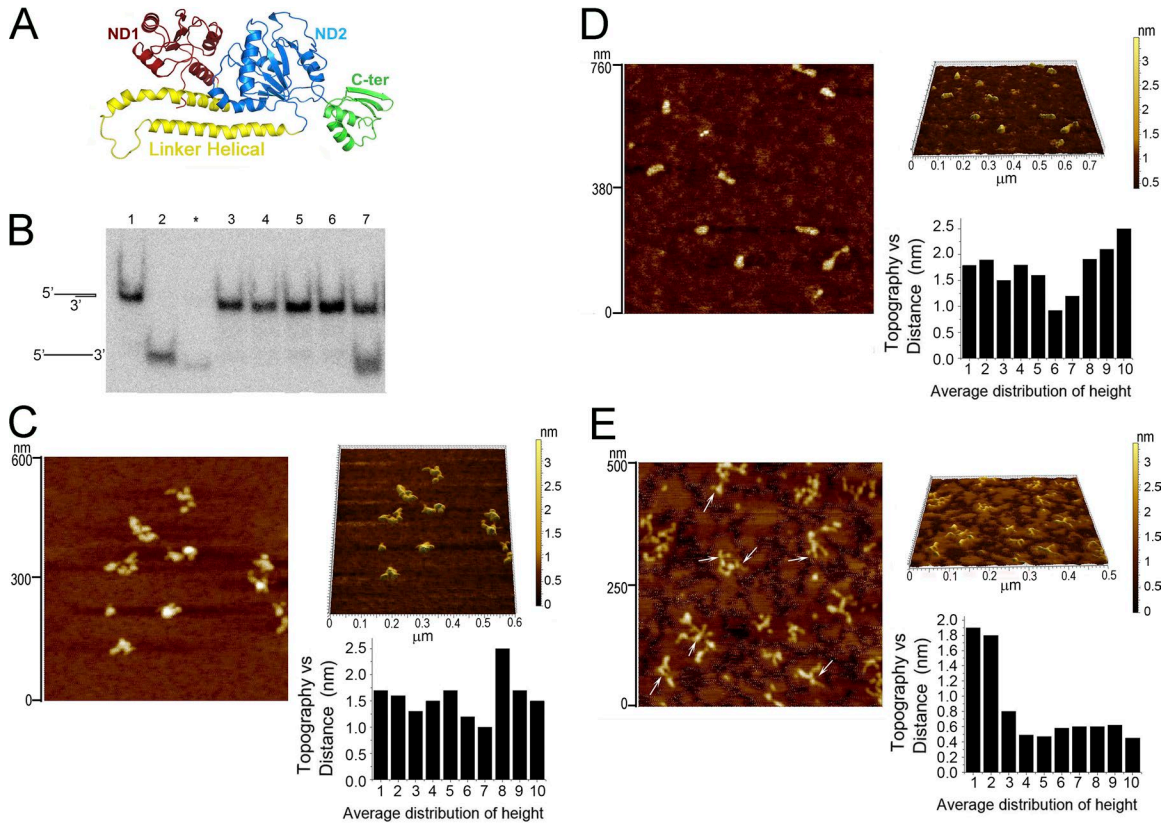

Figure 1. **ATP-dependent RNA helicase activity of *E. coli* HflX. (A)** Different domains of *E. coli* HflX protein (coordinates taken from PDB accession number 5ADY). ND1 (brick red) has been newly characterized as an ATPase domain. ND2 (blue) is the GTPase domain. *E. coli* HflX has an additional C-terminal domain (green). A fork-like helical domain (yellow) connects ND1 and ND2. **(B)** Duplex unwinding by HflX is seen for a 24-nt oligoribonucleotide (in which the self-complementary part is shown) only in presence of ATP. Lane 1, control duplex RNA; lane 2, RNA denatured by heating; lanes 3 and 4, RNA duplex treated with 20 nM and 200 nM HflX, respectively; lanes 5 and 6, treated with 20 nM and 200 nM protein in the presence of GTP; lane 7, treated with 20 nM of protein in the presence of ATP, which shows 45% unwinding of dsRNA (the lane marked with an asterisk is excluded because of spillover from lane 2). **(C and D)** AFM images show that compact structures of large-subunit rRNA molecules (C) are retained even when protein is added without ATP (D). **(E)** In contrast, Y and loop structures (arrows) of unwinding intermediates are seen when protein is added along with ATP. Right panels in C–E show 3D views of the AFM images (up) and mean distribution of molecular heights (bottom). It is clearly seen that although compact structures (C and D) show higher values, height decreases upon duplex unwinding because of single-strand formation (E).

A hallmark of RNA helicases is the ability to couple free energy from ATP hydrolysis to mechanical work used for unwinding of double-stranded RNA (dsRNA). Remarkably, high-salt–washed (partially deformed; Moore et al., 2008; Pulk et al., 2010) as well as heat-shocked 50S subunits showed better ability to stimulate ATP hydrolysis on HflX compared with normal 50S subunit. The fact that ATP on HflX is activated by aberrant form of 50S subunit favors a physiological role of the protein. The combined biochemical and structural results reported in this study support a molecular model in which ND1 of the 50S-bound HflX (in conjunction with the linker helical domain) can modulate heat-inactivated 23S RNA conformation and as a consequence, help in the survival of the bacteria.

Results

HflX manifests RNA helicase activity in an ATP-dependent manner

ND1 has been recognized as ATP-binding domain (Jain et al., 2013). Although a DALI search (an online server for 3D structure comparison of proteins; Holm and Rosenström, 2010) did not show significant structural similarity between ND1 of the *S. solfataricus* HflX crystal structure (Wu et al., 2010) and known ATP-binding domains, when we used ND1 (Fig. 1 A) of the recent cryo-EM structure (Protein Data Bank [PDB] accession number 5ADY) of *E. coli* HflX (bound to the 50S subunit) for our DALI search, several known ATPase domains were identified (Table S1). Intriguingly, consideration of the ND1 along with the linker helical domain for the DALI search displayed an ATP-dependent DNA helicase as one of the structural neighbors (Table S1; PDB accession number 4CGZ; Z-score, 2.3; root mean square displacement, ∼4 Å). This observation prompted us to explore the possibility of helicase activity of *E. coli* HflX.

Because HflX is known as a ribosome-binding protein, we analyzed its RNA helicase processivity by performing a duplex unwinding assay. A short 24-nt oligonucleotide, containing a region of self-complementary sequence of 6 bp with a single-stranded overhang of 12 nt at the 5′ end, was used as the substrate. A classical electrophoretic mobility-shift assay clearly exhibited the duplex RNA-unwinding activity of HflX (Figs. 1 B

Downloaded from http://rupress.org/jcb/article-pdf/217/7/2519/1608330/jcb_201711131.pdf by guest on 05 December 2025

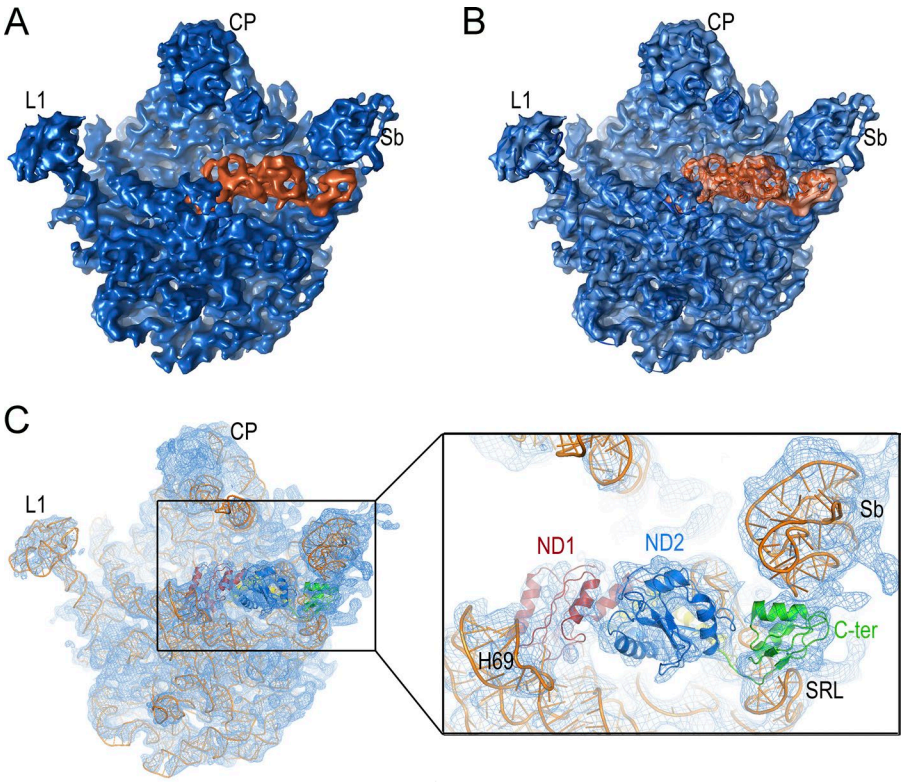

Figure 2. **Cryo-EM 3D reconstruction of the ATP–GTP complex. (A)** Surface representation of cryo-EM density map of the HflX (in the presence of AMP–PNP–GMP–PNP) –bound 50S subunit (blue), with HflX (orange). **(B)** Quasiatomic structure (generated by a flexible fitting approach) matches well with the features of the density maps of the ligand as well as the 50S subunit. The cryo-EM maps are rendered semitransparent for better visualization of the fitted model. **(C)** Cartoon representation of the atomic models of the 50S subunit rRNA (yellow-orange) and HflX fitted inside the density map of the complex (blue mesh) are shown. Close-up view of the bound protein at right shows that the domain features match well with the density attributed to the protein. Domains are colored according to Fig. 1 A. Landmarks for the 50S subunit: CP, central protuberance; L1, L1 protein stalk; Sb, L7/L12 stalk base; SRL, sarcin-rich loop.

and S1 A). RNA helicases frequently function in an ATP-dependent manner. Indeed, the result shows that only ATP stimulates HflX's unwinding activity on the dsRNA substrate, whereas GTP has no effect. Mg^{2+} ion is known to play a critical role for ATPases (Henn et al., 2008). Inhibition of helicase activity in the presence of EDTA suggests involvement of Mg^{2+} ions (Fig. S1 B).

To understand the significance of HflX's RNA helicase activity in the context of ribosome function, we visualized the unwinding catalysis of HflX on large-subunit rRNA using high-resolution AFM imaging (Fig. 1; cryo-EM visualization was also done; Fig. S3 G). AFM imaging provided a means of directly visualizing unwinding catalysis at single-molecule resolution (Henn et al., 2001). Purified rRNA from the 50S subunit was incubated with the protein in the presence or absence of ATP and visualized by AFM. Our AFM results demonstrate that HflX can bind and unwind large-subunit rRNA in an ATP-dependent manner (Fig. 1, C–E). The rRNA molecules were seen (Fig. 1 C) in condensed form (mean height distribution of the molecules 0.8–2 nm). In the absence of ATP, HflX was apparently bound to RNA, but no unwinding catalysis was observed (Fig. 1 D). In contrast, treatment of rRNA with HflX along with ATP clearly showed single-stranded RNA intermediates (single strand height, 0.6 nm; Fig. 1 E). The AFM images showed (Fig. 1 E) several Y-shaped structures (arms comprising two single-stranded RNA regions and a base formed by dsRNA) representing intermediates trapped during unwinding process. Some loop-like structures (created by local strand separation upon unwinding) were also detected. Binding of the protein at the strand-opening junction of the RNA could be identified from an increased height value (~1.4 nm). However, in contrast with the conventional helicases showing directional movement along a nucleic acid strand, HflX apparently functions in a localized manner.

HflX-bound 50S subunit structures reveal the mode of HflX's function

Recent cryo-EM structure of the 50S subunit–bound *E. coli* HflX in the presence of GTP (GMP-PNP; Zhang et al., 2015) has revealed the binding site for HflX on the 50S subunit. To gain further insight into the mechanism of the ATP-dependent helicase action of HflX, we applied cryo-EM and single-particle reconstruction techniques for structural analysis of the 50S-bound HflX complex in the presence of both ATP and GTP (nonhydrolyzable analogues).

The HflX-bound 50S subunit complex in the presence of nonhydrolyzable nucleotides (AMP–PNP and GMP–PNP) was purified using cosedimentation, followed by density gradient separation. The 3D cryo-EM map of the 50S–HflX–ATP–GTP complex (designated in this study as the ATP–GTP complex; gold standard resolution, ~8 Å; Fig. S3 A) was generated (Fig. 2 A). Using a flexible fitting approach, a quasiatomic model of the HflX-bound 50S subunit complex was generated (Fig. 2 B). The resolution of the map was reasonably good for molecular interpretation with the help of the atomic model (Trabuco et al., 2008).

The recent cryo-EM structure of the 50S–HflX–GMP–PNP complex (hereafter GTP complex) described interaction of different domains with the 50S subunit (Zhang et al., 2015). The overall arrangements of different domains in our ATP–GTP complex (Fig. 2 C) appeared to be very similar to that of the GTP complex, indicating that HflX's binding site on the 50S subunit is specific. The 50S–HflX complex in the presence of only AMP–PNP was also gradient purified. The 3D cryo-EM map of that 50S–HflX–AMP–PNP complex (hereafter ATP complex) showed weaker density of the protein on the map (Fig. S3 D), indicating that GTP is likely required for tight association of the protein

Downloaded from http://rupress.org/jcb/article-pdf/217/7/2519/1608330/jcb_201711131.pdf by guest on 05 December 2025

with the 50S subunit. Western blot analysis of the gradient-purified 50S–HflX complexes, showing higher affinity of the protein when GTP is present along with ATP, further corroborates this postulation (Fig. S1, F and G). Differential binding of HflX to the 50S subunit in the presence or absence of nucleotides also confirmed the association of nucleotides with the protein in the complexes we purified.

Close inspection of the arrangements of HflX's different domains revealed that the ND2 and C-terminal domains remained in similar conformation in our complex (Figs. 3 A and S4), as seen in the GTP complex (PDB accession number 5ADY). In contrast, ND1 and the linker helical domain in particular showed substantial conformational changes (Fig. 3, A, D, and E) in the ATP–GTP complex when compared with the GTP complex, indicating the presence of ATP in ND1. Furthermore, a previous study has elucidated that in the presence of both nucleotides, ND2 accommodates GTP, whereas ND1 binds to ATP (Jain et al., 2013). Thus, it is conceivable that nucleotides are bound to HflX in a similar manner on our map. In the GTP complex, GTP was present on ND2 and ND1 was in apo conformation (Zhang et al., 2015). The apo form of ND1 may be considered to be in a conformation similar to the ADP-bound form (Fig. 3 C). Thus, observed ND1 conformational changes can be considered to occur because of ATP hydrolysis (Fig. 3 D). Interestingly, it is clearly visible that a stretch of density connected the linker helical domain to the P-loop region of domain V rRNA in the ATP–GTP complex (Fig. 3 B), whereas no density was seen in the corresponding region of the GTP complex (Fig. 3 C). A similar stretch of density attributable to the linker helical domain is visible in the ATP complex as well (Fig. S3 F). Although the RNA unwinding activity of HflX seems to be nonspecific, the specific binding site of HflX on the 50S subunit fosters the view that the substrate for its helicase activity is likely the region of 23S rRNA, where ND1 is placed.

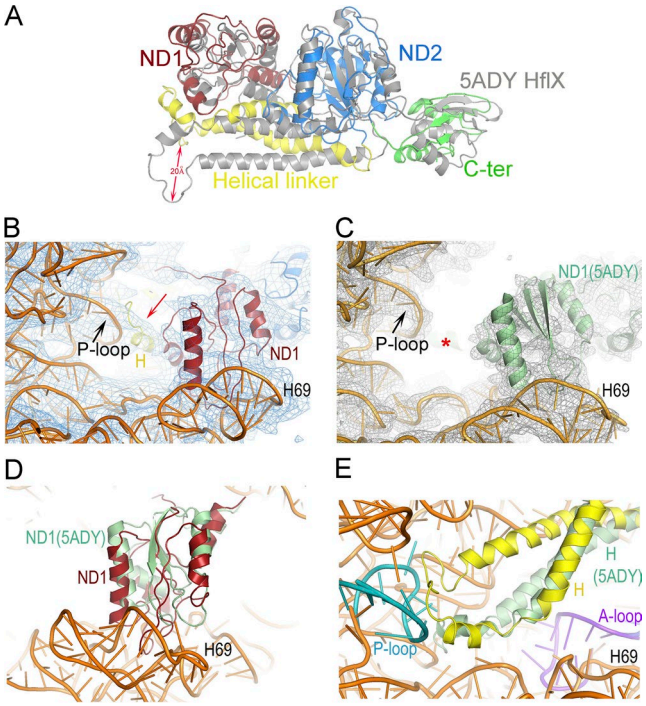

Figure 3. **Interactions of different domains of HflX with the 50S subunit. (A)** Superimposition of the atomic model of HflX fitted into the ATP–GTP complex with the HflX (gray) model of the GTP complex (PDB accession number 5ADY). Different domains of HflX bound to the ATP–GTP complex are shown according to Fig. 1 A. **(B)** The linker helical domain reaching to the PTC shows connecting density in the ATP–GTP complex (red arrow). **(C)** The connection is clearly missing in the GTP complex previously published (Electron Microscopy Data Bank accession number 3133). The region is marked with an asterisk. **(D and E)** Superimposition of the atomic models shows that the ND1 is more inclined toward H69 in the ATP–GTP complex (brick red) compared with its position in the GTP complex (D; pale green), and the linker helical domain in ATP–GTP complex (E; yellow) lies close to the P-loop, whereas it moves away from the P-loop (~20 Å) in the GTP complex (pale green).

Allosteric action of the HflX's linker helical domain in RNA unwinding

We observed that the linker helical domain directly interacted with the domain V region of 23S rRNA in the ATP–GTP complex, and drastic movement of this domain was detected when compared with its conformation in the GTP complex. It appeared that the linker helical domain has a determinant role in eliciting RNA unwinding activity.

To check the RNA helicase activity of ND1 in the presence or absence of the linker helical domain, we made two ND1 constructs: (1) G-domain (ND2) and C-terminal domain deleted (ΔGC); and (2) ND1 only (ND1ΔH; Fig. 4 A). RNA unwinding activity was investigated using an electrophoretic mobility-shift assay, which clearly demonstrated that although ND1 with linker helical domain (ΔGC) showed RNA unwinding activity, ND1 without the linker helical domain (ND1ΔH) could not function as RNA helicase (Figs. 4 B and S1 C). Notably, ATP-dependent helicase activity of ΔGC further confirmed that ATP does bind to ND1.

To further elucidate the helicase activity of ND1 with the linker helical domain (ΔGC), AFM visualization was performed using domain V of 23S rRNA as the substrate. Although ensembles of double strands (height ≥1 nm) or higher-order structures (height ~1.8 nm) were seen when only domain V was visualized (Figs. 4 C and S2 A), the AFM image manifested (Fig. S2, B and C) clear formation of single strands (height 0.4 nm) in the presence of full-length protein. Formation of Y and loop structures displayed (Fig. 4 D) a double-strand (~0.8 nm) opening (0.4 nm) when the linker helical domain was present (ΔGC). In contrast, in the absence of linker helical domain (ND1ΔH), rRNA remained mostly in higher-order structures (Fig. 4 E). No trace of the strand opening was seen. Association of the truncated protein at the Y fork junction can be identified by the increase in height (~1 nm). However, the helicase activity of the full protein on domain V rRNA was more prominent, suggesting that a tightly controlled crosstalk is likely present among the domains (Figs. 4 A and S2). This postulation is supported by the observation (Wu et al., 2010; Jain et al., 2013) that a salt bridge between ND1 and ND2 is crucial for regulating the function of these domains.

HflX rescues heat-shocked ribosomes and boosts cell survival

RNA helicases perform ubiquitous functional roles in regulating RNA biology in vivo (Jankowsky, 2011). We aimed to understand exactly what role HflX plays as an RNA helicase in a cellular context. Recent studies have implicated HflX's function during heat stress (Zhang et al., 2015; Coatham et al., 2016). Data presented

Downloaded from http://rupress.org/jcb/article-pdf/217/7/2519/1608330/jcb_201711131.pdf by guest on 05 December 2025

in one of the previous studies (Zhang et al., 2015) have shown that although heat stress causes damage to normal *E. coli* cells to some extent, it is more detrimental to cells from HflX-deleted strains. To check whether HflX's RNA helicase activity has any additional effect under heat shock, we first sought to understand the role of HflX in cell survival during heat stress. For this assay, we took untransformed BL21 cells (as a control) and three types of plasmid-transformed BL21 cells (full-length HflX, ΔGC, and ND1ΔH in pET28∞). We observed that when the cells were subjected to heat shock (50°C for 40 min) and then plated on Luria-Bertani (LB) growth medium, the growth of untransformed BL21 was severely impaired (Fig. 5 A, row b), whereas IPTG-induced transformed cells with full length HflX survived well (Fig. 5 A, row c). More interestingly, after heat shock, although growth of ND1ΔH transformed cells was impeded (Fig. 5 A, row e), ΔGC transformed cells showed better survival potency compared with untransformed BL21 cells, although the survivability was not as good as it was for the transformed cells containing full-length protein (Fig. 5 A, row d). The effect seen for ΔGC-transformed cells suggests that the ND1, along with the linker helical domain, must have an instrumental role in rescuing heat-damaged cells.

Next, we performed in vitro translation assay (using a T7 in vitro transcription translation kit). Although addition of normal 70S ribosomes to a kit master mix overshot normal production of luciferase (measured as luminescence) by the ribosomes available in a kit master mix, when heat-shocked ribosomes (incubated at 50°C for 40 min) were added to the assay reaction set, protein availability was drastically reduced compared with normal reaction set (Fig. 5 B). Interestingly, when heat-shocked ribosomes were incubated along with HflX before addition to a kit master mix, the production of luciferase increased significantly (Fig. 5 B). The reduction of luciferase production after the addition of heat-shocked ribosomes indicates that the heat-shocked ribosomes are likely nonfunctional and that random distribution of mRNA to functional and nonfunctional ribosomes presumably reduces the efficiency of protein synthesis. However, recovery of enzyme production upon addition of heat-shocked ribosomes along with HflX suggests that HflX must have rescued heat-damaged 70S ribosomes into functional forms. This experiment was repeated using 30S and 50S subunits instead of 70S ribosomes (Fig. 5 C). Interestingly, supply of HflX along with normal 30S and heat-shocked 50S subunits resulted higher luciferase production than kit control, presumably because in this case, splitting of impaired 70S ribosomes by HflX was not required. Addition of normal 30S and heat-shocked 50S subunits produced slightly better luciferase activity. The presence of additional normal 30S subunits most likely increases the probability of normal 70S ribosome availability. It should be noted here that equal amounts of ATP and GTP were added in all reaction sets.

HflX's ATPase activity is stimulated by an aberrant form of the 50S subunit

We observed that like many putative RNA helicases, the RNA-unwinding activity of HflX is ATP dependent (Fig. 1 B). Thus, it is logical to assume that deformed ribosome, being the substrate of the RNA helicase, would be more effective in stimulating ATP

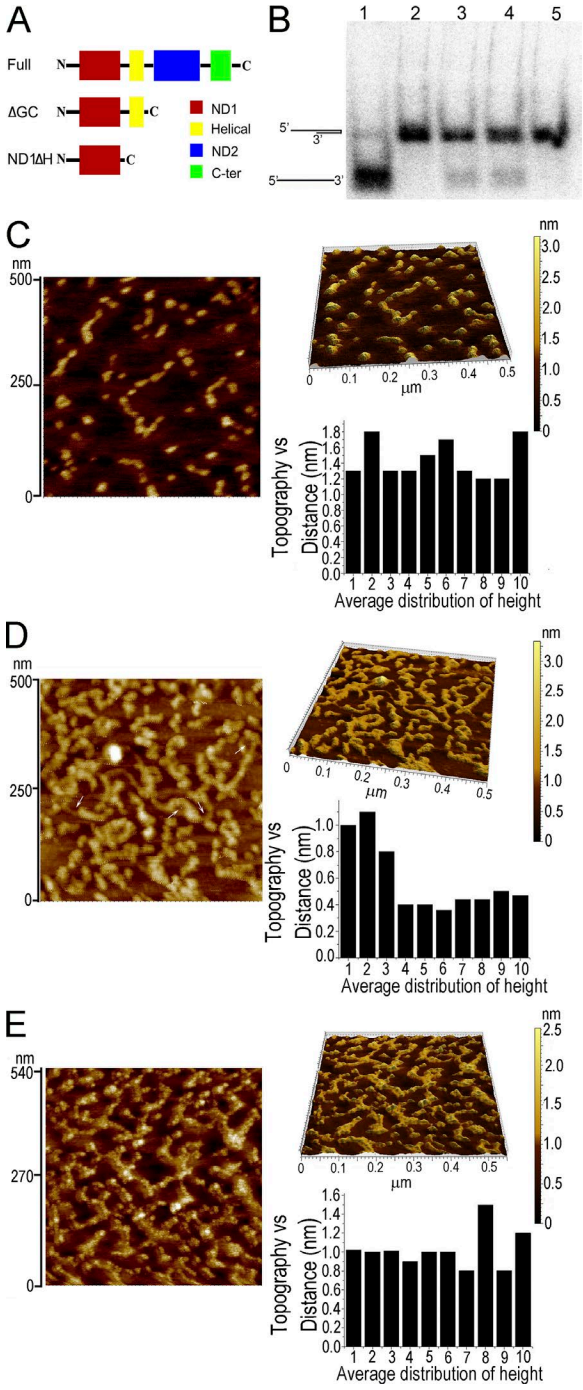

Figure 4. **Role of the linker helical domain of HflX in RNA-unwinding activity. (A)** Graphical representations of full-length HflX and different constructs (ΔGC and ND1ΔH) are shown. **(B)** Assay for helicase activity of different constructs of HflX (using 24-nt oligoribonucleotide) in presence of ATP shows that although ΔGC is capable of unwinding duplex RNA, ND1ΔH is not. Lane 1, RNA denatured by heating; lane 2, control duplex RNA; lanes 3 and 4, RNA duplex treated with 40 nM and 80 nM ΔGC (in the presence of ATP), respectively, and show 11% and 13% unwinding of dsRNA; lane 5, treated with 80 nM ND1ΔH (in the presence of ATP). **(C–E)** AFM images show the compact domain V rRNA structures (C) open up after treatment with ΔGC (D), whereas no trace of unwinding is seen (right) when treated with ND1ΔH (E). Formation of single-stranded structures after ΔGC treatment is detected by a decrease in mean molecular heights (E, right, bottom). 3D representations of the images are shown on the right (top). ATP is present for the treatments shown in D and E.

Downloaded from http://rupress.org/jcb/article-pdf/217/7/2519/1608330/jcb_201711131.pdf by guest on 05 December 2025

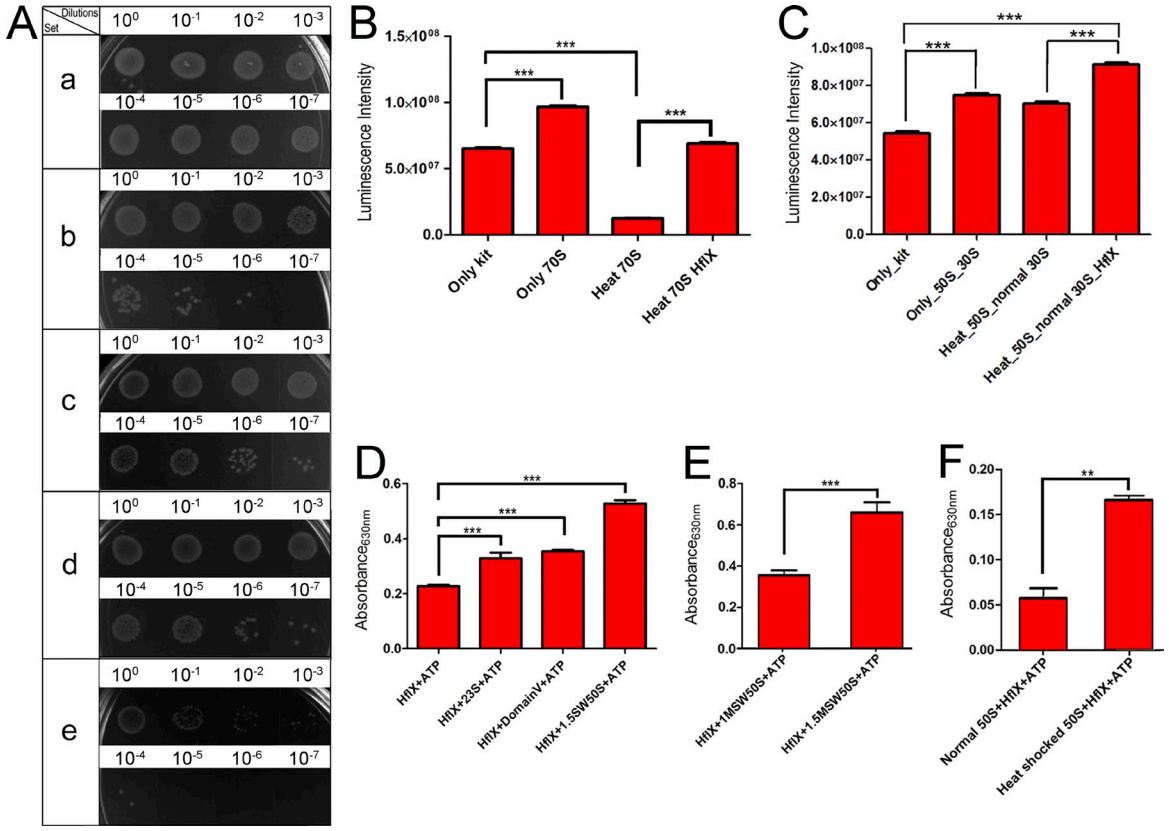

Figure 5. **Effect of ATP-dependent helicase activity of HflX after heat shock. (A)** Growth assay in serial dilution shows that although BL21 (untransformed) grew well (a), heat stress significantly reduced growth of these cells (b), and in HflX (full length)–transformed BL21, heat-shocked cells regained survivability when HflX was induced by IPTG (c). ΔGC construct transformed BL21 cells induced by IPTG showed intermediate survivability to that seen in d and e upon heat shock, whereas ND1ΔH-transformed BL21 cells are highly susceptible to heat shock. **(B)** In vitro transcription/translation assay shows that when normal 70S ribosomes were added to the master mix, luciferase activity (luminescence was measured) increased, but addition of heat-shocked 70S ribosomes drastically reduced enzyme activity. Availability of the enzyme was recovered when HflX was added along with the heat-shocked ribosomes. **(C)** Similar results were found when 30S and 50S subunits were used instead of 70S ribosome. When normal 50S and 30S ribosomal subunits were added to the master mix, luciferase activity increased, but addition of heat-shocked 50S subunit and normal 30S subunit slightly reduced enzyme activity. Enzyme production was enhanced when HflX was added along with the heat-shocked 50S subunit and normal 30S subunit. An equal amount of nucleotides was added in all reaction sets. **(D)** RNA-induced ATPase activity of HflX using a malachite green assay shows that although purified large-subunit rRNA and domain V released more free phosphate compared with autohydrolysis on the protein, the high-salt wash ribosome (partially deformed) showed maximum catalysis, suggesting that ribosome-associated deformed rRNA is more effective than rRNA in isolation. **(E)** The observation of the high-salt–washed 50S subunit catalyzing ATP hydrolysis more than normal 50S subunit in the presence of HflX again suggests that the aberrant form of the 50S subunit is the actual substrate. **(F)** A similar result was found when the effect of heat-shocked 50S subunit on ATP hydrolysis was compared with normal 50S subunit, confirming that heat shock does result in damage to the 50S subunit. Data are presented as means ± SEM (**, P < 0.01; ***, P < 0.001; one-way ANOVA; *n* = 4; statistically significant differences from control).

hydrolysis on HflX. In an effort to verify this presumption, we used a high-salt wash 50S subunit as a mimic of aberrant form of the 50S subunit. High-salt wash (1.5 M) treatment causes detachment of some large subunit proteins (Fig. S1 D). Ribosomal proteins are involved in stabilizing the rRNA structure (Homann and Nierhaus, 1971). It has been shown that high-salt wash results in an inactive (loss of peptidyl transferase activity) 50S subunit (Moore et al., 2008; Pulk et al., 2010). Also, isolated large-subunit rRNA as well as domain V of 23S rRNA may be considered to have improper folding.

We have performed free phosphate determination using malachite green assay (Lanzetta et al., 1979; Baykov et al., 1988) in the presence of domain V, 50S-rRNA, and high-salt wash 50S subunit. After stopping the enzyme reaction, the P_i release upon ATP hydrolysis was estimated by spectrophotometric measurement. The assay clearly showed that the rRNAs effectively stimulated ATPase activity of HflX (Fig. 5 D). However, the high-salt wash 50S subunits showed higher activity than the rRNAs as well as normal-salt wash (1 M) 50S subunits (Fig. 5 E), indicating that the aberrant conformation of domain V, when part of the 50S subunit, is likely the actual substrate. A similar phosphate release assay revealed that the heat-shocked 50S subunits catalyzed ATP hydrolysis better than normal 50S subunits (Fig. 5 F), confirming that heat treatment indeed damages the 50S subunit, which acts as better substrate for ATPase activity on HflX.

Discussion

HflX has recently been described as a heat shock protein (Zhang et al., 2015). It was proposed that HflX splits 70S ribosomes and stabilizes 50S subunits by binding as an antiassociation factor during heat stress. Nevertheless, our biochemical and cell-based assays

Downloaded from http://rupress.org/jcb/article-pdf/217/7/2519/1608330/jcb_201711131.pdf by guest on 05 December 2025

clearly show that in addition to the previously proposed function, RNA helicase activity of HflX is important in rescuing heat-damaged 50S subunit where the linker helical domain of HflX has a profound role in allosterically modulating rRNA structures. In connection to our observation, it may be noted that DNA binds to a helical domain of the Bloom syndrome helicase (Newman et al., 2015), with which structural similarity of HflX was identified by a DALI search. A recent study also suggests a prong-like helical domain in Sen1 (an RNA/DNA helicase) is a critical determinant for its duplex-unwinding activity (Leonaitė et al., 2017).

Most of the bacterial ribosome–related RNA helicases identified so far seem to work under cold stress (Owttrim, 2013; Jarmoskaite and Russell, 2014), when RNA may have a tendency to get kinetically trapped in nonnative conformations (local minima). Under heat stress, however, RNAs, fluctuating between different conformations may encounter difficulty specifying a thermodynamically favored single folded structure over other conformations and thus may need the assistance of RNA helicases (Jankowsky, 2011; Owttrim, 2013). Resolution limitation of the cryo-EM map did not allow us to pinpoint the exact rRNA location where the modulation by HflX occurs. However, in the ATP–GTP complex, the linker helical domain of HflX reaches out to a location of domain V of 23S rRNA harboring the peptidyl transferase center (PTC), and radical movement of this domain was identified when two structures were compared. It is tempting to propose that PTC rRNA is a potential substrate for the RNA helicase action of HflX. It has been known for decades that maturation of PTC is one of the last events to occur during large-subunit assembly (Nierhaus, 1982; Fuller-Pace et al., 1993; Jomaa et al., 2014; Davis et al., 2016). It is possible that this region is the most vulnerable to heat stress and thus requires the assistance of an RNA helicase to recover its active conformation for biological functions.

Based on our results, a model is proposed (Fig. 6) to explain how HflX may function as a modulator of aberrant rRNA conformation after heat shock. ND1, in ATP-bound form, is supposed to be in an active high-energy state ("on" state) and seems to act as a compressed spring when the linker helical domain remains fastened to the rRNA (as seen in the ATP–GTP complex). After ATP hydrolysis, ND1 relaxes and the thrust of the spring opening forces the linker helical domain to move ∼20 Å (to a position seen in the GTP complex). Concomitantly, the rRNA is stretched to unwind and instantly released to rearrange.

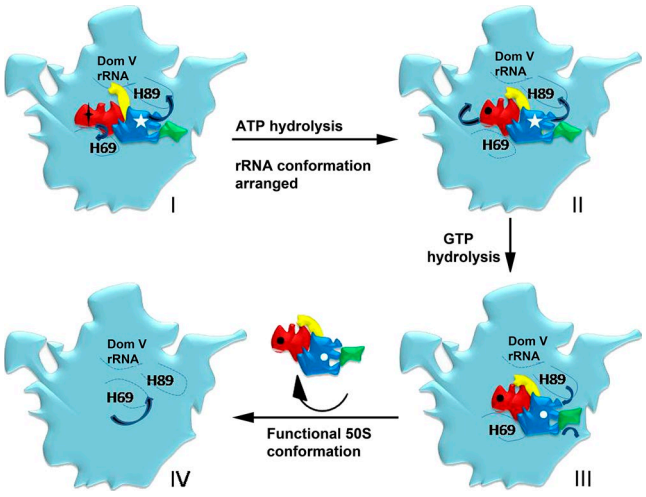

Figure 6. **Proposed sequence of events for HflX's action in modulating rRNA conformation of heat-damaged 50S subunit.** Overall conformation of HflX (in the presence of ATP and GTP) bound to the heat-inactivated 50S subunit. ND1 (red) in ATP-bound (black asterisk) form is inclined toward H69, the linker helical domain (Dom; yellow) grabs the deformed rRNA of domain V, and ND2 in GTP-bound (white asterisk) form leans onto H89 (state I). Conformational changes occur in ND1 after ATP hydrolysis (ADP; black circle). Coupled conformational change in the linker helical domain forces it to move away (20 Å), releasing PTC to unwind and rewind in rightly folded form (state II). Thus, the linker helical domain has an allosteric effect on modulating damaged rRNA conformation. According to a previous structural study (Zhang et al., 2015), presence of the 30S-preinitiation complex stimulates GTP hydrolysis (GDP; white circle) on ND2. After GTP hydrolysis, along with ND2, conformational changes occur in the C-terminal domain (state III). Functional significance of the flexibility of C-terminal domain was proposed by Coatham et al. (2016). The thrust resulting from the C-terminal domain conformational change allows for the release of the protein to produce an active 50S subunit (state IV).

Materials and methods

Purification of the *E. coli* 50S ribosomal subunit and rRNAs

50S subunits were isolated from *E. coli* MRE600 cells. First, 70S ribosomes were purified from log phase (OD_{600} 0.65) growth culture following standard protocols (Traub and Nomura, 1968; Ghosh and Moore, 1979; Das et al., 1996). The 70S ribosomes were split into 50S and 30S subunits in low-Mg^{2+} TMA buffer (20 mM Tris-HCl, pH 7.5, 30 mM NH_4Cl, 0.5 mM $Mg(OAc)_2$, and 5 mM 2-mercaptoethanol). 50S and 30S subunits mixture was centrifuged for 10 h at 140,000 relative centrifugal force (rcf) through 10–40% sucrose gradient. 50S subunits containing fractions were pooled together and sucrose was removed by buffer (20 mM Tris-Cl, pH 7.5, 30 mM NH_4Cl, 10 mM $Mg(OAc)_2$, and 5 mM 2-mercaptoethanol) exchange through a 100-kD cutoff Amicon-Ultra filtration unit.

rRNA (23S and 5S rRNA) of large subunits was isolated from 50S ribosomal subunits using TRIzol and a Thermo Fisher Scientific RNA isolation kit. After TRIzol-dependent RNA isolation, the RNA pellet was washed two times with ice-cold 75% ethanol at 12,000 rcf for 5 min at 4°C. After washing, the pellet was dried carefully and dissolved in nuclease-free water (Amresco). The rRNA pool was then purified again using the Thermo Fisher Scientific RNA isolation kit protocol (the 260/280 ratio was 1.99).

The domain V region of 23S rRNA sequence containing DNA (a gift from C. Barat, St. Xavier's College [Autonomous], Kolkata, India) was cloned in pTZ57R/T after the T7 promoter site. To produce domain V rRNA, we used the Thermo Fisher Scientific in vitro transcription system. First, the construct was linearized using EcoR1 endonuclease. The in vitro transcription process was performed using T7 RNA polymerase (Thermo Fisher Scientific) and ribonucleotides (Thermo Fisher Scientific). 1 U/20 µl DNase was added to the mixture and incubated for 15 min at room temperature. Half of the volume of reaction mixture of 7 M ammonium acetate and 2.5 times the total volume of ice-cold ethanol were then added and incubated overnight at −80°C. The sample was centrifuged at 12,000 rcf for 30 min, and the supernatant

Downloaded from http://rupress.org/jcb/article-pdf/217/7/2519/1608330/jcb_201711131.pdf by guest on 05 December 2025

was discarded. The RNA pellet was washed two times with ice-cold 75% ethanol at 12,000 rcf for 15 min at 4°C. After washing, the pellet was dried and nuclease free water (Amresco) was added to dissolve RNA (the 260/280 ratio was 2).

Protein purification:

The *E. coli* HflX construct (pET28∞ plasmid with HflX gene inserted; a gift from B. Prakash, Indian Institute of Technology, Kanpur, India) was transformed to *E. coli* BL21 cells (Jain et al., 2009, 2013). Cell culture of log phase (OD_{600} = 0.6) was induced with 0.6 mM IPTG (Sigma-Aldrich) for 10 h at 26°C. Cells were harvested and lysed in lysis buffer (20 mM Tris-HCl, pH 7.6, 500 mM NaCl, 5% glycerol, 2 mM 2-mercaptoethanol, 1 mM PMSF, and 5 mM imidazole) by ultrasonication. After centrifugation of cell lysates at 12,000 rcf for 30 min at 4°C, the supernatant was loaded onto a column containing Ni-Sephadex beads (GE Healthcare), washed with wash buffer (20 mM Tris-HCl, pH 7.6, 500 mM NaCl, 5% glycerol, 1 mM PMSF, 2 mM 2-mercaptoethanol, and 40 mM imidazole) and eluted with elution buffer (20 mM Tris-HCl, pH 7.6, 500 mM NaCl, 5% glycerol, 1 mM PMSF, 2 mM 2-mercaptoethanol, and 250 mM imidazole). HflX-containing fractions were pooled together, buffer exchanged with storage buffer (20 mM Tris-HCl, pH 7.6, 500 mM NaCl, 5% glycerol, and 5 mM 2-mercaptoethanol), and concentrated using an Amicon ultra 30 kD filtration unit. HflX proteins (confirmed by standard mass spectrometry analysis [MALDI-TOF-TOF-4800; Applied Biosystems]) were divided into aliquots and stored at −80°C.

Gene sequences of two truncated protein forms (ND1 with the linker helical domain, G and C terminal domains deletion of HflX [ΔGC], and ND1 only, without the linker helical domain [ND1ΔH]) were inserted into the pET28∞ plasmid and transformed into BL21 cells (done separately). The purification procedure for these two truncated proteins (ΔGC and ND1ΔH) was the same as that used for HflX protein, except that the pH 6.9 buffer was used for ΔGC (a list of primers is given in Table S2). The SDS-PAGE gel showed the quality of purified proteins (Fig. S1 E).

Protein-binding assay

We prepared two complexes: (1) 50S–HflX–AMP–PNP–GMP–PNP and other was 50S–HflX–AMP–PNP. To make these complexes, proteins and 50S subunits were incubated at a ratio of 23:1. First, proteins were incubated with either 5 mM AMP-PNP (Sigma-Aldrich) only or both 5 mM AMP–PNP (Sigma-Aldrich) and 4 mM GMP–PNP for 20 min at 4°C (in respect to reaction volume). 50S subunits were mixed with analogue-bound proteins in binding buffer (20 mM Tris-Cl, pH 7.6, 50 mM NH_4Cl, 10 mM $Mg(OAc)_2$, and 1 mM DTT) for 45 min at 4°C and then loaded on the sucrose gradient (10% to 40%). Ultracentrifugation was done at 140,000 rcf for 6 h at 4°C, and the gradient was then analyzed at 260 nm. Subunits containing fractions were pooled together, and sucrose was removed by binding buffer exchanged through a 100-kD cut-off Amicon-Ultra filtration unit. The sample was then separated on SDS-PAGE gel to confirm HflX binding.

RNA helicase assay

The RNA-unwinding activity of HflX, ΔGC, and ND1ΔH was performed following published protocols (Henn et al., 2001; Chandran et al., 2007) with minor modifications. A 24-nt oligoribonucleotide (Trilink) with the sequence 5′-GAAUGUACA UCAGAGUGCGCACUC-3′ was used for the helicase assay in which the underlined part of the sequence is self-complementary. The oligonucleotide was phosphorylated with T4 polynucleotide kinase (Fermentas) and gamma-[^{32}P]-ATP and separated from unincorporated isotopes on a Sephadex G-25 column (Roche). Labeled oligonucleotides were further purified using the TRIzol method and precipitated with an equal volume of isopropyl alcohol at −20°C overnight, and the pellet was resuspended in 50 µl hybridization buffer (20 mM Tris–HCl, pH 7.5, and 500 mM NaCl). Before the gel separation assay, oligonucleotide solution was incubated at 95°C for 4 min and then slowly cooled to room temperature. RNA-unwinding activity was performed in vitro by measuring the conversion of self-duplex RNA to single-stranded RNA. For this assay, purified protein was incubated with 6 fmol (0.1 nM) of duplex RNA in a 50-µl reaction volume containing 20 mM Tris–HCl, pH 7.5, 5 mM $MgCl_2$, 60 mM KCl, 5% (vol/vol) glycerol, 100 ng yeast tRNA, 50 U RNasin (Promega), and 2 mM nucleotide triphosphate (ATP or GTP). Full-length HflX along with ΔGC and ND1ΔH truncated proteins were used in this assay. In the case of ΔGC, pH 6.9 was used for the reaction buffer and 5 mM and 10 mM ATP were used to examine ATP dependency. First, RNA and protein were kept at 4°C for 20 min. The reaction mixture was then incubated at 37°C for 30 min, after which the reaction was stopped by adding 50 µl 2× stop buffer (20% glycerol, 0.2% SDS, 4 mM EDTA, 0.025% bromophenol blue, and 0.025% xylene cyanol). 20 µl reaction mixture was analyzed directly by electrophoresis on a native 12% polyacrylamide gel (29:1) in 0.5× Tris-borate-EDTA buffer. The gel was dried and visualized using a Phosphorimager. GelQuantNET software (Biochem Lab Solutions) was used to evaluate the band intensities.

Cell survivability assay

For this assay, we used untransformed BL21 cells as WT cells and three types of plasmid (HflX full protein, ΔGC, and ΔH in Pet28∞)–transformed BL21 cells. Overnight-grown cells were added to new LB growth media to reach OD_{600} 0.6, and then an equal amount of cells were taken for induction (0.1 mM IPTG was used for induction at 27°C for 1 h), pelleted, and washed twice. The same number of cells was used to induce heat shock. Heat shock was done at 50°C for 40 min, after which cells were plated on LB with serial dilution and kept at 30°C for 18 h.

In vitro translation assay

We used the T7 in vitro transcription–translation kit to assay the role of HflX on heat-stressed ribosomes. A luciferase template (supplied by the kit) was used in every reaction set. Luciferase production was measured by activity of luciferase in a luminometer. To give heat shock to ribosomes, ribosomes were incubated at 50°C for 40 min and then immediately transferred onto ice. To repair the heat-stressed ribosomes by using HflX, 2 nM heat-stressed ribosomes (70S or 50S subunits), 0.6 mM ATP, and 0.6 mM GTP were incubated with 50 nM HflX at 4°C for 20 min and then transferred at 37°C for 30 min. After that, the reaction mixture was added to the kit master mix and incubated at 37°C for 90 min. 0.6 mM ATP and 0.6 mM GTP were maintained in

Downloaded from http://rupress.org/jcb/article-pdf/217/7/2519/1608330/jcb_201711131.pdf by guest on 05 December 2025

all reaction sets including the control set. For heat-treated subunits (50S), 2 nM normal 30S subunits was added to the master mix. To estimate the presence of active luciferase enzyme, luciferase activity was measured in a luminometer; 50 µl luciferin (Promega) and 2.5 µl reaction mixture were mixed, and luminescence was measured using a Glomax 20/20 luminometer (the integration time was 10 s).

Assessment of ATPase activity

ATPase activity was determined using a malachite green assay (Lanzetta et al., 1979; Baykov et al., 1988; Wu et al., 2009; with slight modification). The ATP hydrolysis reaction was performed by incubating 20 µM HflX with 1 mM ATP, rRNA of 50S subunits or domain V rRNA or high-salt (1.5 M)–washed 50S subunit (100 nM for each) or heat-treated 1 M salt-washed 50S subunit (1 µM) in a buffer containing 50 mM Tris–HCl, pH 8.0, 200 mM NaCl, 1 mM 2-mercaptoethanol, and 5 mM $MgCl_2$ at 37°C for 60 min in 25 µl reaction volume. After 1 h, 125 µl of 1× reaction buffer was added to increase the reaction volume to 150 µl. A filtration step was performed to remove protein and RNA from reaction mixture using 30-kD cutoff filtration units (Sartorius). To determine ATP hydrolysis, a malachite green–ammonium molybdate mixture was used. Concentrated sulfuric acid (d = 1.84 g/l) was added to 300 ml double-distilled water, and 0.44 g malachite green was then mixed in (Baykov et al., 1988). After that, 2.5 ml of 7.5% ammonium molybdate and 0.2 ml of 11% Tween-20 were added to 10 ml malachite green solution and kept at room temperature for 60 min (orange). This mixture was then filtered through a 0.22-µm syringe filter just before use. The ATP hydrolysis reaction was stopped by adding the malachite green–ammonium molybdate mixture in a 4:1 ratio (sample, malachite green–ammonium molybdate mixture) and incubated for 5 min at room temperature (green). Finally, 25 µl of 34% citric acid solution (for 100 µl reaction mixture) was added (Lanzetta et al., 1979) and incubated for 2 min at room temperature, and absorbance was measured at 630 nm.

Western blot analysis

We did Western blot experiments to compare the binding efficiency of HflX protein with the 50S subunit in the presence of AMP–PNP only, both AMP–PNP and GMP–PNP, and without any nonhydrolyzing analogue. 50S subunits and a two-times molar volume of HflX protein were incubated in binding buffer (20 mM Tris-HCl, pH 7.6, 50 mM NH_4Cl, 10 mM $Mg(OAc)_2$, and 1 mM DTT) at 4°C for 45 min, and the reaction mixture was separated through a 10% to 40% sucrose gradient by using ultracentrifugation at 140,000 rcf for 5 h The gradient was then fractionated, absorbance was measured at 260 nm, and the 50S subunit–containing fraction pooled and filtered using 100-kD filtration units to remove sucrose. Sample concentration was measured at 260 nm, and an equal amount of sample was separated on SDS-PAGE and processed for Western blotting.

We used Western blot experiments to quantify the total HflX protein concentration including cloned HflX protein and native HflX protein in BL21 cells containing HflX construct, compared with BL21 cells without HflX construct after 50°C for 40 min of heat shock. In these experiments, OD_{260} 0.2 1 ml cell culture was used for heat shock and SDS-PAGE gel separation. Cells lysis and SDS-PAGE sample preparation were done according to a published protocol (Zhang et al., 2015).

Western blot analysis was performed to quantify the bound HflX protein concentration. Blots were probed with anti–His antibody or anti–HflX antibody (Biobharati Lifescience). Binding of the secondary HRP-conjugated anti–rabbit antibodies (EMD Millipore) was analyzed using ImmunoCruz (Santa Cruz Biotechnology, Inc.). Intensities were measured using gel-quant-net software.

Sample preparation for AFM

Freshly cleaved mica was incubated with 3-aminopropyl triethoxysilane (Sigma-Aldrich) before applying samples (Lyubchenko and Shlyakhtenko, 1997). In AFM experiments, rRNA of the 50S subunits and domain V RNA were incubated in reaction buffer A (20 mM Hepes, pH 7.5, 50 mM NH_4Cl, and 5 mM $MgCl_2$), heated at 95°C for 4 min, and then slowly cooled to room temperature. Either free RNA or protein–RNA solution was deposited on freshly treated mica for 5 min at room temperature, rinsed with water, and dried. HflX and domain V rRNA (1:2 ratio) were incubated in reaction buffer A containing 0.5 mM DTT for 30 min at 37°C. The final concentration of ATP was 10 mM.

AFM for visualizing helicase activity

We primarily followed the procedure described previously (Henn et al., 2001). AFM experiments were performed in intermittent contact mode (called "tapping" or AAC mode) to minimize tip-induced damage. AAC mode AFM was performed using a Pico plus 5500 inverted light microscope AFM (Agilent Technologies) with a Piezo scanner (maximum range 9 µm). Microfabricated silicon cantilevers 225 µm in length with a nominal spring force constant of 21–98 N/m were used (Nano Sensors). Cantilever oscillation frequency was tuned into resonance frequency. The cantilever resonance frequency was 150–300 kHz. The images (512 × 512 pixels) were captured with a scan size between 0.5 and 0.8 µm at a scan speed rate of 0.5 lines/s. Images were processed by flatten using Pico view1.1 version software (Agilent Technologies). Image manipulation was done using Pico Image Advanced version software (Agilent Technologies).

Cryo-EM and 3D image processing

Grids for cryo-EM were prepared following standard procedures using Vitrobot Mark IV (FEI; Grassucci et al., 2007). Micrographs were recorded on a Philips FEI POLARA field emission gun electron microscope operated at 300 kV equipped with a low-dose kit and an Oxford cryo-transfer holder at a total magnification of 79,894×. Data were collected using 4,000 × 4,000 Eagle charge-coupled device Camera (FEI) with a physical pixel size of 15 µm (corresponding with a pixel size of 1.89 Å on the object scale) and defocus values ranging from 1.0–4.8 µm. All images were acquired using low-dose procedures with an estimated dose of ∼20 electrons/$Å^2$. SPIDER (Frank et al., 1996; Shaikh et al., 2008) and EMAN2 (Tang et al., 2007) were used for image processing.

Cryo-EM image processing and model building

Good micrographs were selected after inspection of drift, astigmatism, and the presence of Thon rings in the power spectrum.

Downloaded from http://rupress.org/jcb/article-pdf/217/7/2519/1608330/jcb_201711131.pdf by guest on 05 December 2025

Particles were picked by SPIDER auto picking (Rath and Frank, 2004) using an empty 50S cryo-EM density map as reference model (filtered to very low resolution), and from auto-picked particles, good particles were selected manually. Image processing using SPIDER included a 3D projection alignment procedure with correction of the contrast transfer function. Using small number of particles (~14,000), a cryo-EM 3D map was generated, which was subsequently used as the initial model in EMAN2 3D reconstruction.

Particles were stacked and imported to EMAN2 for 3D reconstruction. Three cryo-EM density maps were generated (the control 50S subunit, the 50S–HflX–AMP–PNP–GMP–PNP complex [ATP–GTP complex], and the 50S–HflX–AMP–PNP [ATP complex]) using 57,759, 61,557, and 32,159 final sets of particles, respectively. The gold-standard resolutions of the resultant maps were 11.7 Å, 8.1 Å, and 14.8 Å, respectively. To generate a quasi-atomic model of the complex, available atomic structure was fitted into EM map. The structure of 50S-bound HflX taken from PDB accession number 5ADY (removed GTP) was fitted into the attributable cryo-EM density isolated from the 3D map of the 50S–HflX–AMP–PNP–GMP–PNP complex, followed by molecular dynamics flexible fitting (Trabuco et al., 2008). Cross-correlation coefficients were measured for the fitted domains using VMD and Chimera (Pettersen et al., 2004). Chimera and PyMol (Delano Scientific) were used for structural analysis and to prepare illustrations.

For sample preparation to visualize helicase activity in cryo–transmission EM, large-subunit rRNA was incubated with HflX protein (2:1) in reaction buffer (20 mM Hepes, pH 7.5, 50 mM NH_4Cl, 5 mM $MgCl_2$, 10 mM ATP, and 0.5 mM DTT) at 4°C for 20 min and then kept at 37°C for 30 min.

Accession numbers

The cryo-EM density map of the 50S–HflX–ATP–GTP complex has been deposited in the Electron Microscopy Data Bank (EMD-6979). The fitted atomic model has been deposited in the PDB (5ZZM).

Online supplemental material

Fig. S1 shows purification of different constructs of HflX and their RNA-unwinding activity. Fig. S2 shows AFM visualizations of nucleotide-dependent unwinding of domain V of 23S rRNA by HflX. Fig. S3 presents cryo-EM maps of control and ATP complexes and resolutions of the maps. Fig. S4 shows close-up views of different domains of HflX fitted into the cryo-EM map of the ATP–GTP complex. Table S1 presents results of the DALI search. Table S2 lists the primer sequences.

Acknowledgments

Technical assistance provided by Mr. T. Muruganandan and Mr. Sandip Chakraborty during the AFM experiments and mass spectrometry analysis is gratefully acknowledged. We are grateful to Dr. Ilic Zoran (Wadsworth Center, Albany, NY) for critically checking the manuscript. We sincerely thank Mr. S. Krishnamoorthi, Ms. Priya Das, Mr. Saurav Verma, and Ms. T. Anusha for assisting with several experiments, protein purification, and preliminary cryo-EM data processing. We thank Dr. Balaji Prakash and Dr. Chandana Barat for the gifts of E. coli HflX protein and domain V constructs.

This work was supported by the Council of Scientific and Industrial Research (India) Network project UNSEEN (BSC0113), the Science and Engineering Research Board (Department of Science and Technology, India)–sponsored project GAP327, and Council of Scientific and Industrial Research – Indian Institute of Chemical Biology (Kolkata, India). Funding provided by the National Institute of Pharmaceutical Education and Research, India, for project students is gratefully acknowledged. S. Dey acknowledges University Grants Commission, India, for Senior Research Fellowship.

The authors declare no competing financial interests.

Author contributions: J. Sengupta conceived the idea. S. Dey and J. Sengupta designed the experiments. S. Dey carried out bulk of the biochemical and AFM experiments and cryo-EM 3D image processing. S. Dey and J. Sengupta analyzed the data. C. Biswas performed cryo grid preparation, cryo-EM data collection, and preliminary analysis of the dataset. J. Sengupta wrote the paper with help from S. Dey.

Submitted: 20 November 2017
Revised: 26 March 2018
Accepted: 14 May 2018

References

Ash, M.R., M.J. Maher, J. Mitchell Guss, and M. Jormakka. 2012. The cation-dependent G-proteins: in a class of their own. *FEBS Lett.* 586:2218–2224. https://doi.org/10.1016/j.febslet.2012.06.030

Baykov, A.A., O.A. Evtushenko, and S.M. Avaeva. 1988. A malachite green procedure for orthophosphate determination and its use in alkaline phosphatase-based enzyme immunoassay. *Anal. Biochem.* 171:266–270. https://doi.org/10.1016/0003-2697(88)90484-8

Blombach, F., H. Launay, V. Zorraquino, D.C. Swarts, L.D. Cabrita, D. Benelli, J. Christodoulou, P. Londei, and J. van der Oost. 2011. An HflX-type GTPase from Sulfolobus solfataricus binds to the 50S ribosomal subunit in all nucleotide-bound states. *J. Bacteriol.* 193:2861–2867. https://doi.org/10.1128/JB.01552-10

Britton, R.A. 2009. Role of GTPases in bacterial ribosome assembly. *Annu. Rev. Microbiol.* 63:155–176. https://doi.org/10.1146/annurev.micro.091208.073225

Caldon, C.E., and P.E. March. 2003. Function of the universally conserved bacterial GTPases. *Curr. Opin. Microbiol.* 6:135–139. https://doi.org/10.1016/S1369-5274(03)00037-7

Chandran, V., L. Poljak, N.F. Vanzo, A. Leroy, R.N. Miguel, J. Fernandez-Recio, J. Parkinson, C. Burns, A.J. Carpousis, and B.F. Luisi. 2007. Recognition and cooperation between the ATP-dependent RNA helicase RhlB and ribonuclease RNase E. *J. Mol. Biol.* 367:113–132. https://doi.org/10.1016/j.jmb.2006.12.014

Coatham, M.L., H.E. Brandon, J.J. Fischer, T. Schümmer, and H.J. Wieden. 2016. The conserved GTPase HflX is a ribosome splitting factor that binds to the E-site of the bacterial ribosome. *Nucleic Acids Res.* 44:1952–1961. https://doi.org/10.1093/nar/gkv1524

Das, B., S. Chattopadhyay, A.K. Bera, and C. Dasgupta. 1996. In vitro protein folding by ribosomes from Escherichia coli, wheat germ and rat liver: the role of the 50S particle and its 23S rRNA. *Eur. J. Biochem.* 235:613–621. https://doi.org/10.1111/j.1432-1033.1996.00613.x

Davis, J.H., Y.Z. Tan, B. Carragher, C.S. Potter, D. Lyumkis, and J.R. Williamson. 2016. Modular Assembly of the Bacterial Large Ribosomal Subunit. *Cell.* 167:1610–1622.

Dutta, D., K. Bandyopadhyay, A.B. Datta, A.A. Sardesai, and P. Parrack. 2009. Properties of HflX, an enigmatic protein from Escherichia coli. *J. Bacteriol.* 191:2307–2314. https://doi.org/10.1128/JB.01353-08

Downloaded from http://rupress.org/jcb/article-pdf/217/7/2519/1608330/jcb_201711131.pdf by guest on 05 December 2025

Frank, J., M. Radermacher, P. Penczek, J. Zhu, Y. Li, M. Ladjadj, and A. Leith. 1996. SPIDER and WEB: processing and visualization of images in 3D electron microscopy and related fields. *J. Struct. Biol.* 116:190–199. https://doi.org/10.1006/jsbi.1996.0030

Fuller-Pace, F.V., S.M. Nicol, A.D. Reid, and D.P. Lane. 1993. DbpA: a DEAD box protein specifically activated by 23s rRNA. *EMBO J.* 12:3619–3626.

Ghosh, N., and P.B. Moore. 1979. An investigation of the conformational properties of ribosomes using N-ethylmaleimide as a probe. *Eur. J. Biochem.* 93:147–156. https://doi.org/10.1111/j.1432-1033.1979.tb12805.x

Grassucci, R.A., D.J. Taylor, and J. Frank. 2007. Preparation of macromolecular complexes for cryo-electron microscopy. *Nat. Protoc.* 2:3239–3246. https://doi.org/10.1038/nprot.2007.452

Henn, A., O. Medalia, S.P. Shi, M. Steinberg, F. Franceschi, and I. Sagi. 2001. Visualization of unwinding activity of duplex RNA by DbpA, a DEAD box helicase, at single-molecule resolution by atomic force microscopy. *Proc. Natl. Acad. Sci. USA.* 98:5007–5012. https://doi.org/10.1073/pnas.071372498

Henn, A., W. Cao, D.D. Hackney, and E.M. De La Cruz. 2008. The ATPase cycle mechanism of the DEAD-box rRNA helicase, DbpA. *J. Mol. Biol.* 377:193–205. https://doi.org/10.1016/j.jmb.2007.12.046

Holm, L., and P. Rosenström. 2010. Dali server: conservation mapping in 3D. *Nucleic Acids Res.* 38:W545-9. https://doi.org/10.1093/nar/gkq366

Homann, H.E., and K.H. Nierhaus. 1971. Ribosomal proteins. Protein compositions of biosynthetic precursors and artifical subparticles from ribosomal subunits in Escherichia coli K 12. *Eur. J. Biochem.* 20:249–257. https://doi.org/10.1111/j.1432-1033.1971.tb01388.x

Huang, B., H. Wu, N. Hao, F. Blombach, J. van der Oost, X. Li, X.C. Zhang, and Z. Rao. 2010. Functional study on GTP hydrolysis by the GTP-binding protein from Sulfolobus solfataricus, a member of the HflX family. *J. Biochem.* 148:103–113. https://doi.org/10.1093/jb/mvq039

Jain, N., N. Dhimole, A.R. Khan, D. De, S.K. Tomar, M. Sajish, D. Dutta, P. Parrack, and B. Prakash. 2009. E. coli HflX interacts with 50S ribosomal subunits in presence of nucleotides. *Biochem. Biophys. Res. Commun.* 379:201–205. https://doi.org/10.1016/j.bbrc.2008.12.072

Jain, N., N. Vithani, A. Rafay, and B. Prakash. 2013. Identification and characterization of a hitherto unknown nucleotide-binding domain and an intricate interdomain regulation in HflX-a ribosome binding GTPase. *Nucleic Acids Res.* 41:9557–9569. https://doi.org/10.1093/nar/gkt705

Jankowsky, E. 2011. RNA helicases at work: binding and rearranging. *Trends Biochem. Sci.* 36:19–29. https://doi.org/10.1016/j.tibs.2010.07.008

Jarmoskaite, I., and R. Russell. 2014. RNA helicase proteins as chaperones and remodelers. *Annu. Rev. Biochem.* 83:697–725. https://doi.org/10.1146/annurev-biochem-060713-035546

Jomaa, A., N. Jain, J.H. Davis, J.R. Williamson, R.A. Britton, and J. Ortega. 2014. Functional domains of the 50S subunit mature late in the assembly process. *Nucleic Acids Res.* 42:3419–3435. https://doi.org/10.1093/nar/gkt1295

Lanzetta, P.A., L.J. Alvarez, P.S. Reinach, and O.A. Candia. 1979. An improved assay for nanomole amounts of inorganic phosphate. *Anal. Biochem.* 100:95–97. https://doi.org/10.1016/0003-2697(79)90115-5

Leipe, D.D., Y.I. Wolf, E.V. Koonin, and L. Aravind. 2002. Classification and evolution of P-loop GTPases and related ATPases. *J. Mol. Biol.* 317:41–72. https://doi.org/10.1006/jmbi.2001.5378

Leonaitė, B., Z. Han, J. Basquin, F. Bonneau, D. Libri, O. Porrua, and E. Conti. 2017. Sen1 has unique structural features grafted on the architecture of the Upf1-like helicase family. *EMBO J.* 36:1590–1604. https://doi.org/10.15252/embj.201696174

Lyubchenko, Y.L., and L.S. Shlyakhtenko. 1997. Visualization of supercoiled DNA with atomic force microscopy in situ. *Proc. Natl. Acad. Sci. USA.* 94:496–501. https://doi.org/10.1073/pnas.94.2.496

Moore, S.D., T.A. Baker, and R.T. Sauer. 2008. Forced extraction of targeted components from complex macromolecular assemblies. *Proc. Natl. Acad. Sci. USA.* 105:11685–11690. https://doi.org/10.1073/pnas.0805633105

Newman, J.A., P. Savitsky, C.K. Allerston, A.H. Bizard, Ö. Özer, K. Sarlós, Y. Liu, E. Pardon, J. Steyaert, I.D. Hickson, and O. Gileadi. 2015. Crystal structure of the Bloom's syndrome helicase indicates a role for the HRDC domain in conformational changes. *Nucleic Acids Res.* 43:5221–5235. https://doi.org/10.1093/nar/gkv373

Nierhaus, K.H. 1982. Structure, assembly, and function of ribosomes. Curr. Top. *Microbiol. Immunol.* 97:81–155.

Noble, J.A., M.A. Innis, E.V. Koonin, K.E. Rudd, F. Banuett, and I. Herskowitz. 1993. The Escherichia coli hflA locus encodes a putative GTP-binding protein and two membrane proteins, one of which contains a protease-like domain. *Proc. Natl. Acad. Sci. USA.* 90:10866–10870. https://doi.org/10.1073/pnas.90.22.10866

Owttrim, G.W. 2013. RNA helicases: diverse roles in prokaryotic response to abiotic stress. RNA Biol. 10:96–110. https://doi.org/10.4161/rna.22638

Pettersen, E.F., T.D. Goddard, C.C. Huang, G.S. Couch, D.M. Greenblatt, E.C. Meng, and T.E. Ferrin. 2004. UCSF Chimera--a visualization system for exploratory research and analysis. *J. Comput. Chem.* 25:1605–1612. https://doi.org/10.1002/jcc.20084

Pulk, A., A. Liiv, L. Peil, U. Maiväli, K. Nierhaus, and J. Remme. 2010. Ribosome reactivation by replacement of damaged proteins. *Mol. Microbiol.* 75:801–814. https://doi.org/10.1111/j.1365-2958.2009.07002.x

Rath, B.K., and J. Frank. 2004. Fast automatic particle picking from cryo-electron micrographs using a locally normalized cross-correlation function: a case study. *J. Struct. Biol.* 145:84–90. https://doi.org/10.1016/j.jsb.2003.11.015

Sato, A., G. Kobayashi, H. Hayashi, H. Yoshida, A. Wada, M. Maeda, S. Hiraga, K. Takeyasu, and C. Wada. 2005. The GTP binding protein Obg homolog ObgE is involved in ribosome maturation. *Genes Cells.* 10:393–408. https://doi.org/10.1111/j.1365-2443.2005.00851.x

Schaefer, L., W.C. Uicker, C. Wicker-Planquart, A.E. Foucher, J.M. Jault, and R.A. Britton. 2006. Multiple GTPases participate in the assembly of the large ribosomal subunit in Bacillus subtilis. *J. Bacteriol.* 188:8252–8258. https://doi.org/10.1128/JB.01213-06

Shaikh, T.R., R. Trujillo, J.S. LeBarron, W.T. Baxter, and J. Frank. 2008. Particle-verification for single-particle, reference-based reconstruction using multivariate data analysis and classification. *J. Struct. Biol.* 164:41–48. https://doi.org/10.1016/j.jsb.2008.06.006

Shields, M.J., J.J. Fischer, and H.J. Wieden. 2009. Toward understanding the function of the universally conserved GTPase HflX from Escherichia coli: a kinetic approach. *Biochemistry.* 48:10793–10802. https://doi.org/10.1021/bi901074h

Tang, G., L. Peng, P.R. Baldwin, D.S. Mann, W. Jiang, I. Rees, and S.J. Ludtke. 2007. EMAN2: an extensible image processing suite for electron microscopy. *J. Struct. Biol.* 157:38–46. https://doi.org/10.1016/j.jsb.2006.05.009

Trabuco, L.G., E. Villa, K. Mitra, J. Frank, and K. Schulten. 2008. Flexible fitting of atomic structures into electron microscopy maps using molecular dynamics. *Structure.* 16:673–683. https://doi.org/10.1016/j.str.2008.03.005

Traub, P., and M. Nomura. 1968. Structure and function of Escherichia coli ribosomes. I. Partial fractionation of the functionally active ribosomal proteins and reconstitution of artificial subribosomal particles. *J. Mol. Biol.* 34:575–593. https://doi.org/10.1016/0022-2836(68)90182-4

Verstraeten, N., M. Fauvart, W. Versées, and J. Michiels. 2011. The universally conserved prokaryotic GTPases. *Microbiol. Mol. Biol. Rev.* 75:507–542. https://doi.org/10.1128/MMBR.00009-11

Wu, H., J. Min, T. Antoshenko, and A.N. Plotnikov. 2009. Crystal structures of human CDY proteins reveal a crotonase-like fold. *Proteins.* 76:1054–1061. https://doi.org/10.1002/prot.22472

Wu, H., L. Sun, F. Blombach, S.J. Brouns, A.P. Snijders, K. Lorenzen, R.H. van den Heuvel, A.J. Heck, S. Fu, X. Li, et al. 2010. Structure of the ribosome associating GTPase HflX. *Proteins.* 78:705–713.

Zhang, Y., C.S. Mandava, W. Cao, X. Li, D. Zhang, N. Li, Y. Zhang, X. Zhang, Y. Qin, K. Mi, et al. 2015. HflX is a ribosome-splitting factor rescuing stalled ribosomes under stress conditions. *Nat. Struct. Mol. Biol.* 22:906–913. https://doi.org/10.1038/nsmb.3103

Downloaded from http://rupress.org/jcb/article-pdf/217/7/2519/1608330/jcb_201711131.pdf by guest on 05 December 2025